Stabilised D_2R G-protein coupled receptor oligomers identify multi-state β-arrestin complexes

Katie L. Sharrocks[1,3], Francesca Fanelli[2], Yewei Lui[1], Annabelle J. Milner[3], Wu Yining[1], Bernadette Byrne[1*], Aylin C. Hanyaloglu[3*]

[1]Department of Life Sciences, Imperial College London, UK

[2]Department Life Sciences, University of Modena and Reggio Emilia, Modena, Italy

[3]Department of Metabolism, Digestion and Reproduction, Imperial College London, UK

*To whom correspondence should be addressed: b.byrne@imperial.ac.uk, a.hanyaloglu@imperial.ac.uk

Keywords: GPCR; D2 dopamine receptor; arrestin; β-arrestin-2; dimer; oligomer; internalization; single-molecule imaging; molecular modelling; MAPK signaling

Abstract

The G-protein coupled receptor (GPCR) superfamily directs central roles in many physiological and pathophysiological processes via diverse and complex mechanisms. GPCRs can exhibit signal pleiotropy via formation of di/oligomers both with themselves and other GPCRs. A deeper understanding of the molecular basis and functional role of oligomerization would facilitate rational design of activity-selective ligands. A structural model of the D2 dopamine receptor (D_2R) homomer identified distinct combinations of substitutions likely to stabilise protomer interactions. Molecular modelling of β-arrestin-2 (βarr2) bound to predicted dimer models suggests a 2:2 receptor:βarr2 stoichiometry, with the dimer favouring βarr2 over Gαi coupling. A combination of biochemical, biophysical and super-resolution, single molecule imaging approaches demonstrated that the D_2R mutant homomers exhibited greater stability. The mutant D_2R homomers also exhibited bias towards recruitment of the GPCR adaptor protein βarr2 with either faster or ligand-independent βarr2 recruitment, increased internalization and reprogrammed ERK signaling compared to D_2R WT. Through GPCR dimer-stabilisation, we demonstrate that D_2R di/oligomerization has a role in βarr2-biased signaling.

Introduction

G-protein coupled receptors (GPCRs) are the largest family of proteins in mammals, are expressed in a range of cell types and regulate a diverse set of physiological processes[1]. They are the targets of approximately 35% of current FDA approved drugs and remain major drug discovery targets[2,3]. Each GPCR can regulate several intracellular signaling cascades through interaction with a range of G-proteins and arrestins[4,5].

Class A 'rhodopsin-like' GPCRs can function as monomers, however increasing biophysical, computational and pharmacological evidence suggests that they can form both homomers and heteromers with other GPCRs[6–13]. A dynamic equilibrium between monomers and transient di/oligomers has been reported for several GPCRs[14–17]. Oligomerization can impact the function of receptors, altering ligand efficacy, G-protein activation or preference for G-protein coupling selectivity[18–21]. The impact of oligomerization on the non-visual arrestins, β-arrestin-1 and 2 (βarr1 and βarr2, respectively, also known as arrestin 2 and 3) is less clear but a recent study showed that oligomerization of platelet-activating factor receptor (PAFR) decreases βarr recruitment and conversely, βarr seemed to decrease oligomerization of the receptor[22]. β_2AR has also been shown to dimerise in a βarr-dependent manner upon stimulation with a βarr-biased ligand[23]. This highlights the potential of oligomerization to dramatically influence all aspects of GPCR signaling.

Structural biology remains an important area for uncovering GPCR activation and dimerization mechanisms[24], yet there have been limited reports of high-resolution structures of class A GPCR dimers/oligomers. According to the limited PDB structures

concerning GPCR dimers, the most recurrent interfaces involve helix 1 (H1). Indeed, H1-H1 contacts were found in homo-dimeric rhodopsin (PDB: 2I36, 2I37, 3CAP, and 6OFJ), κ-opioid (PDB: 4DJH), β1-adrenergic (PDB: 4GPO), M3-muscarinic (PDB: 5ZHP), EP3-prostanoid (PDB: 6AK3), AT1-angiotensin (PDB: 6DO1), and apelin (PDBs 6WOL and 6WON) receptors. Furthermore, H1-H4 contacts were found in homo-dimeric 5HT2A-serotonin (PDBs: 6WGT and 6WH4) and CCR5-chemokine (PDBs: 4MBS and 6AKX) receptors, whereas H1-H5 contacts were found in homo-dimeric D4 dopamine receptor (PDB: 6IQL). Homodimers characterized by H4-H5 or H4-H6 H5-H5, or H6-H7 were found for CXCR4, β1-AR, C5a1, CCR2, α2C-AR and CysLT1 receptors (PDBs: 3ODU/3OE8/3OE9, 5F8U, 5O9H, 6GPX, 6KUW, 6RZ5, respectively).

The D_2 dopamine (D_2R) is a class A 'rhodopsin-like' GPCR, coupling to $G\alpha_{i/o}$[25]. The primary roles of D_2R in the brain are regulation of locomotion and in reward and reinforcement mechanisms[26]. It has been implicated in a number of neurological diseases including schizophrenia and Parkinson's Disease[27]. D_2R has been shown to form homodimers both in heterologous expression systems at physiological expression levels and in native tissues[15,28–30]. Several antipsychotics target the D_2R/βarr2 complex and an increase in D_2R homodimers has been associated with schizophrenia[31,32]. The implication of D_2R complexes in several neurological diseases therefore makes them excellent therapeutic targets.

While there are several high-resolution structures of monomeric D_2R, also in complex with G-protein[33–35], the precise molecular interactions between protomers and the absence of high-resolution dimer structures has hindered the ability to specifically target these complexes for therapeutic benefits.

Here we employed a convergent strategy to engineer distinct stabilised D_2R homodimers. Residues were identified within the H1-H2 interface to enhance homodimer/oligomer stability. Interestingly, these engineered receptors also exhibited a bias towards βarr2 associated pathways with either altered temporal kinetics of ligand-mediated complexes, or functionally biased ligand-independent GPCR/arrestin complexes. Docking of βarr2 to the predicted homodimers of wild type (WT) or mutated D_2R provide insights into the signaling active supramolecular assembly. This may highlight a novel selective role for D_2R homomers in promoting distinct transitions to βarr2 association and signaling activity.

Results

D_2R mutations at the H2-H2 interface increase D_2R homodimer stability and protomer proximity

To stabilise a D_2R homodimer, our experimental design was guided by molecular modelling (see Methods). Simulations of D_2R homodimerization were carried out using the structural models of either the inactive or the active states of the receptor (PDBs: 6CMO and 8IRS, respectively). In all cases, the predicted homodimer forms a symmetrical interface and are characterized by H1-H1, H1-H2 and H2-H2 contacts crowded in the extracellular ends and by a few H1-H8,H8-H8 contacts in the cytosolic side (hereafter indicated as H1,H2 dimer) (Fig. 1a). The stronger contacts from both protomers in the extracellular half of the interface involve: a) Y36 (H1) and F102 (extracellular loop 1 (ECL1)) ; b) T39 (H1) and W90 (H2) and; c) T42 (H1) and I45 (H1) d) V97 (H2) from both protomers; and e) V96 and Y93 (both in H2). We focused on the most extracellular amino acid residues to potentially favour the formation of disulphide bridges in this oxidising environment. To strengthen the contacts between protomers at the interface, our models identified mutations of Y93 to cysteine (Y93C), V96 to either serine (V96S) or cysteine (V96C) and V97 to cysteine (V97C) alone or in combination with V96S (V96S/V97C).

To assess the effect of these mutations on levels of di/oligomeric protein present in cells, western blot analysis under reducing or non-reducing conditions (in the presence or absence of β-mercaptoethanol) was carried out. Under non-reducing conditions all receptors were in a higher order, likely dimeric, complex (>180 KDa) (Fig. 1b). Under reducing conditions, most of the WT D_2R shifted in size predominately to a monomeric form (predicted size of FLAG-tagged D_2R-Rluc8, ~90kDa with glycosylated D_2R-Rluc8

appearing at ~110kDa), however a greater proportion of V96C, V96S and in particular, V96S/V97C mutants, existed in a higher order complex (Fig. 1b-d). Furthermore, BRET saturation assays to measure receptor-receptor interactions in intact cells, confirmed a significant increase in BRETmax in cells transfected with D_2R V96C, V96S or V96S/V97C compared to D_2R WT (Figs. 1e-n), indicating an increase in protomer proximity within a homomer. There was no change in BRET50 (an indicator of protomer-protomer affinity) relative to WT for any of the mutants. Addition of the D_2R selective agonist, quinpirole, did not significantly impact either the BRETmax or BRET50 from BRET saturation curves (Supplementary Fig. 1). This supports the data obtained by western blot analysis, that the V96C, V96S and V96S/V97C mutations may stabilise and/or increase the proportion of D_2R homomers. Computational simulations of V96C (Mut1) and V96S/V97C (Mut2) homodimerization predicted that these mutated homodimers exhibit the same architecture as the WT, though in Mut2 the interface is tighter than in WT or Mut1 (Supplementary Fig. 2). In the predicted Mut1 dimer, C96 interacts with both Y93 and C96 on the facing protomer, whereas in the Mut2 dimer C97 interacts with C97 and S96 interacts with Y93 on the facing protomer.

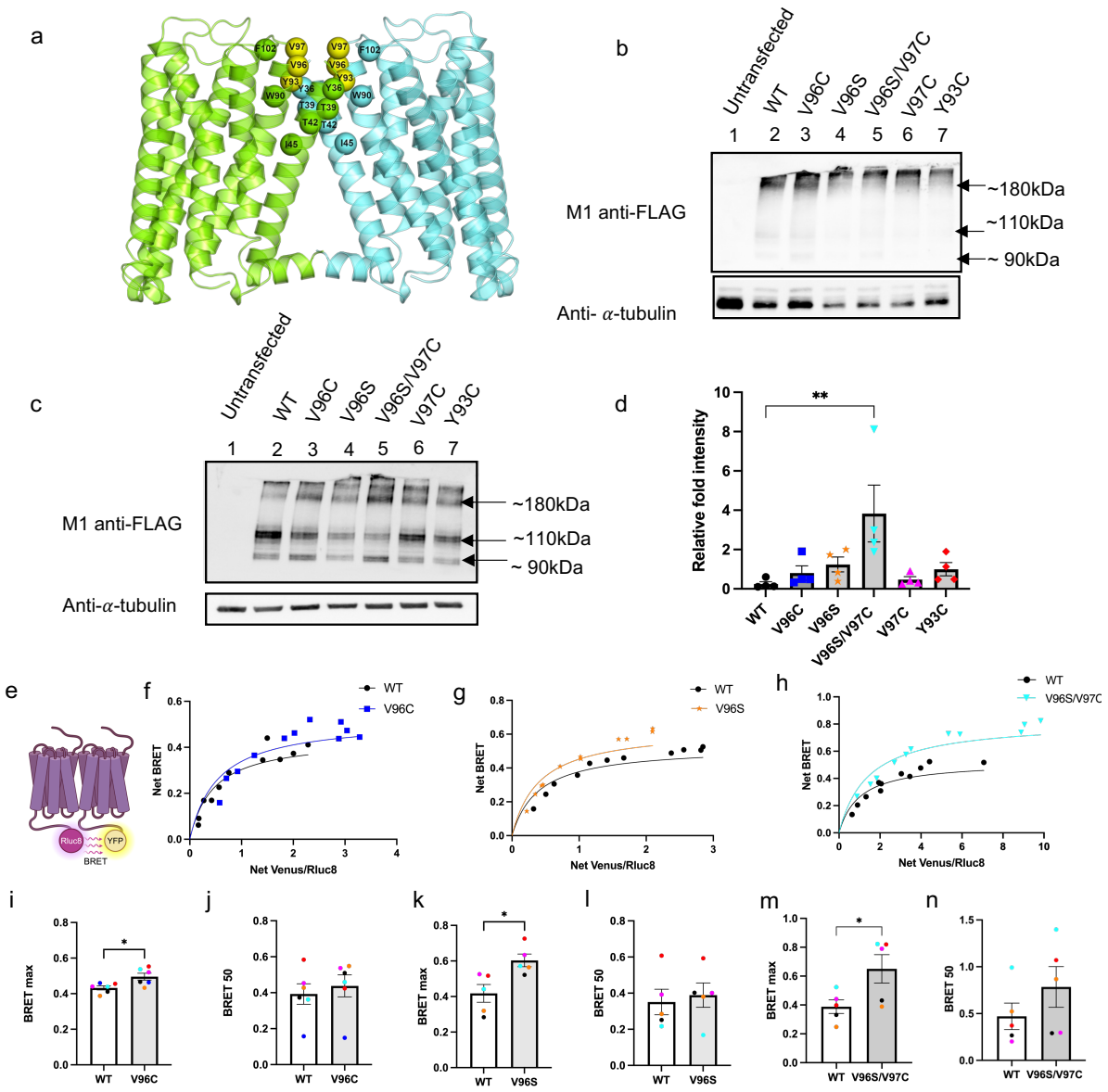

Fig.1. The impact of D_2R mutants identified from molecular docking simulations on homodimer stability. (a) The predicted WT D_2R homodimer is shown in cartoon representation, with the two protomers coloured lemon-green and aquamarine. Interface amino acids are shown as spheres centred on the Cα-atoms. The mutated amino acids are highlighted in yellow. **(b)** Western blot with HEK293 cell lysates transfected with D_2R-Rluc8 WT or mutant constructs, carried out under non-reducing conditions (**b**) and reducing conditions (**c**). Probed with M1 anti-FLAG to detect the FLAG tag at the N-terminus of receptor constructs (D_2R-Rluc8 ~90kDa or ~110kDa with glycosylation) and anti-α-tubulin as a loading control. (**d**) Quantification of western blot band intensity, represented as relative fold change of D_2R dimer levels to monomer levels under reducing conditions, N=4, error bars are +/- SEM. Ordinary one-way ANOVA used to measure statistical differences, (p**=0.0051) (**e**) Schematic showing BRET assay. (**f**) Representative BRET saturation curve obtained from transfection of HEK293 cells with D_2R WT (black) and D_2R V96C (blue) or (**g**) V96S (orange) or **(h)** V96S/V97C constructs (cyan). Saturation curves were used to quantity BRETmax (**i, k, m**) and BRET50 values (**j, l, n**), colour coded for each individual experiment N=5 for WT vs V96S and N=6 for WT vs V96C or V96S/V97C. Un-paired, two-tailed Student's t test used to measure statistical differences in BRET50 or BRETmax values between WT and mutant D_2R, (p*= 0.0186 (i) or 0.0162 (k) or 0.0432 (m)).

Super-resolution imaging of cell surface D_2R at the single molecule level reveals increased oligomerization in D_2R V96S/V97C mutants

Both BRET and Western blot methods assess the total receptor population within a cell, whether in the biosynthetic, plasma membrane, or endocytic compartments. To quantitate the organisation of individual receptors on the plasma membrane, photoactivated localization microscopy with photoactivatable dyes (PD-PALM) with TIRF-imaging was employed. This single-molecule high-resolution technique gives <10 nm resolution and has provided detailed information on plasma membrane localised GPCRs in monomeric, dimeric or oligomeric forms[36–40]. PD-PALM imaging was carried out on HEK 293 cells expressing WT or mutant D_2Rs and directly labelled with an anti-FLAG antibody conjugated to CAGE 500 dye. Precise localisation of individual receptors and subsequent processing through neighbourhood analysis software enabled individual monomer or oligomer populations to be quantified (Fig. 2a and b). Under basal conditions, the percentage of total receptors in a monomeric state in D_2R V96S/V97C cells was significantly lower than WT D_2R (Fig. 2c). Additionally, for V96S/V97C there was an increase in the proportion of receptors in the oligomeric state compared to WT D_2R. When these oligomer populations were assessed according to the number of receptors in the complex, this revealed that these assemblies primarily involved receptor dimers (~17% of associated receptors), yet also a range of higher-order receptor oligomers. The increase in associated V96S/V97C receptor was not attributed to enrichment of a specific oligomer population but rather across receptor di/oligomers (Fig. 2d).

Following quinpirole stimulation, the receptors exhibited distinct propensities in the levels of monomer and oligomeric complexes, compared to basal conditions (Fig. 2e-

g). Stimulation of D_2R WT expressing cells with quinpirole did not significantly alter the proportion of receptors in an oligomeric complex. However, ligand activation of D_2R V96S resulted in a significant decrease in the proportion of receptor in an oligomer compared to both WT D_2R expressing cells stimulated with ligand and D_2R V96S expressing cells in the absence of ligand (Fig. 2e and f). There was also a decrease in the proportion of dimeric receptors relative to WT D_2R (Fig. 2g).

Receptor density can influence oligomerization, and for D_2R specifically the percentage of monomeric receptors was inversely proportional to the receptor density (Supplementary Fig. 3a and b). While for some GPCRs, receptor density impacts higher order complexes (>5 receptors)[40], our observation for D_2Rs via super-resolution imaging is in line with other studies with D_2R_L using diffraction-limited single molecule imaging, reporting a small but significant impact of receptor density on the levels of monomer and di/oligomer distribution[15]. Therefore, based on the correlation observed via PD-PALM analysis, the di/oligomeric state of receptors were also analysed under 'high' (>100 receptors/μM^2) or 'low' (<100 receptors/μM^2) surface receptors, to understand the effect of receptor density on homomer formations in WT and mutant receptors (supplementary Fig. 3b-h). In the absence of agonist, no changes in the trends between WT and mutant D_2Rs due to receptor density were observed. The range of receptor density in cells treated with quinpirole was generally lower for cells expressing D_2R V96S and V96C compared to WT or V96S/V97C, likely due to ligand-induced receptor internalization (Supplementary Fig. 3b). This may partially account for the decrease in oligomeric receptors in D_2R V96S or V96C compared to WT D_2R as when cells with similar receptor densities were analysed, this decrease was not significant (Supplementary Fig. 3g and h).

Taken together, this may suggest that the V96S/V97C mutant increases the propensity for D_2R to form an oligomer. This is in line with docking simulations that predict a tighter interface in the V96S/V97C dimer compared to the WT or the V96C dimer (Supplementary Fig. 2). These results provide further evidence that the V96S/V97C mutant D_2R increases the stability of D_2R oligomers. While, on balance quinpirole stimulation does not significantly alter the organization of D_2R complexes.

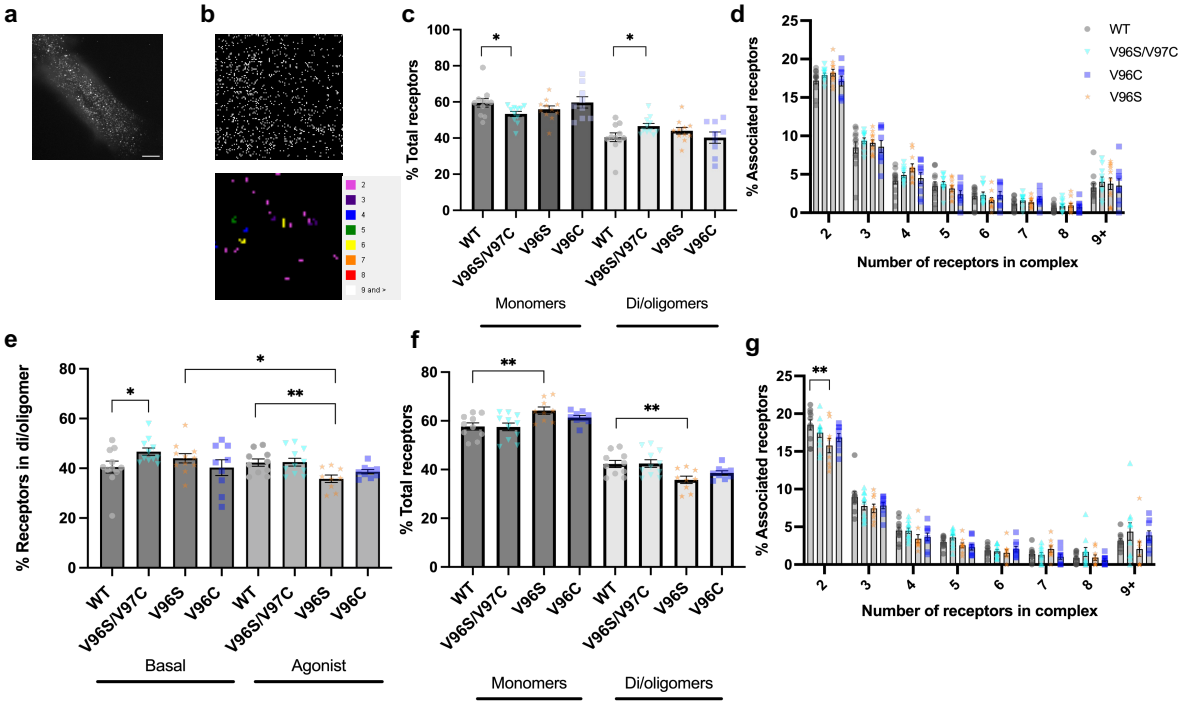

Fig. 2. PD-PALM super-resolution microscopy allows quantification of cell surface D_2R oligomers. (**a**) Representative image HEK293 cells transiently transfected with FLAG-D_2R and labelled with FLAG-CAGE500, imaged over a time course by TIRF microscopy following uncaging and activation of the CAGE500 dye. Scale bar=50 µm. **b)** Representative PD-PALM 7 μm^2 image of FLAG-D_2R labelled with FLAG-CAGE500 with a heat map quantifying oligomer populations. (**c**) Proportion of D_2R WT or mutant receptors as monomers or in di/oligomeric complexes as a percentage of total receptors. (**d**) Composition of D_2R oligomers separated into number of receptors in the complex and expressed as a percentage of total receptors. (**e**) Proportion of associated receptors in di/oligomeric complexes, expressed as a percentage of total number of receptors under basal conditions or after 5 minutes 10 µM quinpirole stimulation. (**f**) Proportion of D_2R WT or mutant receptors as monomers or in di/oligomeric complexes as a percentage of total receptors after 5 minutes 10 µM quinpirole stimulation. (**g**) Composition of D_2R oligomers after 5 minutes 10 µM quinpirole stimulation prior to fixation, separated into number of receptors in the complex and expressed as a percentage of total receptors. Mean +/- SEM, N=3 individual experiments, 3-4 cells imaged for each independent repeat. In c, e and f unpaired, two-tailed Student's t test used to measure differences between WT and mutant D_2R (p*=0.042 (c and e) or 0.0035 p**=0.0068 (e and f)). In d and g two-way ANOVA followed by Šídák's multiple comparisons test used to measure statistical differences between WT and mutant D_2R in different receptor complexes (p**=0.0019).

D_2R mutants that stabilise homomeric interactions impact Gαi-mediated signaling and βarr2 recruitment profiles

Following the observation that some mutations increase the stability of D_2R homomers, the impact of these mutations on canonical Gαi signaling was assessed. Forskolin-induced cAMP levels were measured in the presence of quinpirole to assess inhibition of intracellular cAMP levels due to D_2R signaling. HEK293 cells expressing D_2R WT or V96C and stimulated with 1 μM quinpirole for 5, 15, or 30 minutes exhibited a decrease in forskolin-induced cAMP levels at all agonist time points (Supplementary Fig. 4). This decrease in cAMP is specifically due to D_2R-mediated signaling as untransfected HEK293 cells do not show this decrease upon quinpirole addition. Dose-response curves in D_2R WT or mutant expressing cells showed similar curves and EC_{50} values, suggesting that D_2R mutant receptors show no significant change in potency of quinpirole to activate D_2R and Gαi-mediated signaling pathways (Fig. 3a and Table 1). However, when treated with 100 nM (log-7M) quinpirole, which was taken as the maximal Gαi response, V96S/V97C and V96S mutant D_2Rs had significantly higher cAMP levels compared to WT (Fig. 3b). This suggests that the efficacy of quinpirole to induce D_2R mediated Gαi response is WT-like in V96C, V97C and Y93C transfected cells but lower in cells transfected with D_2R V96S and V96S/V97C.

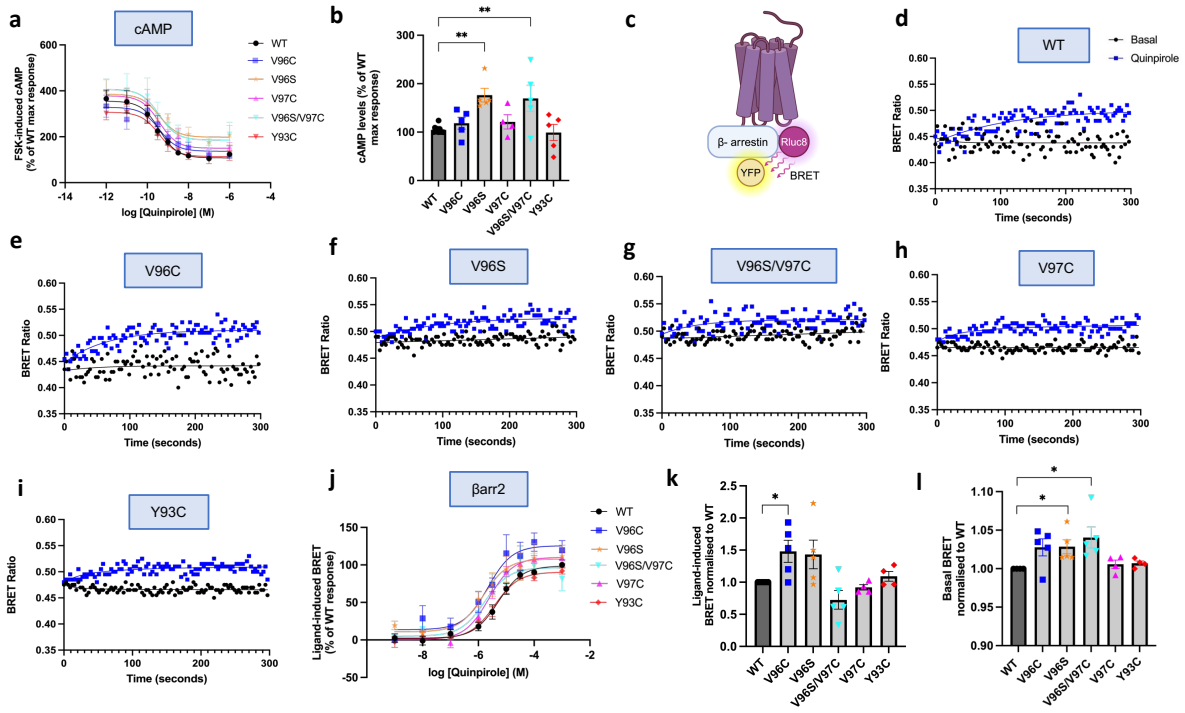

Fig. 3. Altered Gαi-signaling and βarr2 recruitment profiles in D_2R mutants (a) Forskolin-induced cAMP levels as a percentage of maximal response of corresponding D_2R WT, quinpirole dose response curves in D_2R WT (black) or mutant D_2R transfected HEK293 cells. Values plotted are +/- SEM of 4 or 5 independent experiments. (**b**) Plot of cAMP levels when stimulated with 100nM quinpirole, represented as a percentage of WT maximal response. One-way ANOVA and Dunnett's multiple comparisons test used to measure statistical differences between WT and mutant maximal responses (p**= 0.0016(V96S) or 0.0040 (V96S/V97C)) (**c**) Schematic showing BRET assay. Representative kinetic curve showing BRET ratios in HEK293 cells cotransfected with βarr2-YFP and D_2R WT (**d**), V96C (**e**), V96S (**f**), V96S/V97C (**g**), V97C (**h**), Y93C (**i**). Plotted over time for basal (black) and after 10 μM quinpirole stimulation (blue). Graphs representative of 4-6 independent experiments. (**j**) BRET luminescence values were measured before agonist addition and after addition of increasing concentrations of quinpirole, values are average of measurements taken over 5 minutes Represented as a percentage of D_2R WT maximal response, for each individual experiment. Ligand-induced BRET values (**k**) and Basal BRET (**l**) for each individual experiment for cells treated with the maximum dose of quinpirole (1 mM), represented as a fold change from WT. One sample t and Wilcoxon test. N=4-5 +/- SEM. (p*= 0.0488 (k) or 0.0344 or 0.0398).

To assess the impact of these mutant D_2Rs on βarr1/2 recruitment, BRET assays were carried out in HEK293 cells expressing D_2R and βarr1/2. The kinetics of βarr1/2 recruitment were analysed in real time via BRET measured over a time-course of 5 minutes following agonist stimulation. The WT D_2R did not recruit βarr1 following quinpirole treatment (Supplementary Fig. 5a and c). However, in cells expressing D_2R WT and βarr2-YFP there was a rapid increase in BRET levels specifically after quinpirole addition, up to a maximum level of BRET signal which remained stable for at least 5 minutes (Fig. 3d and Supplementary Fig. 6). All D_2R mutants (except for D_2R-Rluc V96S/V97C) showed a similar profile (Fig. 3e-i). The ability of D_2R to couple to βarr2 over βarr1 is consistent with other studies[41,42]. Curve-fitting of the ligand-induced BRET profile allowed quantification of the kinetics of βarr2 recruitment to WT and mutant D_2Rs (Table 2 and Supplementary Fig. 6). There was no significant difference in the plateau of the fitted kinetic profiles between WT or any mutant D_2R, suggesting these mutations do not affect the degree that βarr2 is recruited by D_2R. However, the halftime of the D_2R V96C kinetic curve was significantly lower than WT, suggesting that D_2R V96C recruits βarr2 significantly faster.

Dose-response curves were also carried out to assess the potency of quinpirole to induce βarr2 recruitment to WT or mutant receptors (Fig. 3j-l). D_2R V96C and V96S receptors showed a left shift in the dose-response curves, compared to WT with significantly lower EC_{50} values (Table 1). The other D_2R mutants V97C and Y93C did not show significantly altered dose-response curves. This suggests that in cells expressing the V96C and V96S mutants, quinpirole exhibits increased potency towards βarr2 recruitment. Interestingly, there is a significant increase in basal βarr2 recruitment via BRET in cells transfected with D_2R V96S and V96S/V97C compared

to D_2R WT (Fig. 3l). Combined with the reduced ligand-induced BRET signal in kinetic assays (Fig. 3), this may suggest increased constitutive association between the V96S/V97C receptor and βarr2.

Overall, this data suggests that V96C, and to some extent V96S, have faster kinetics and/ or increased quinpirole-induced βarr2 recruitment to D_2R, while V96S/V97C exhibits enhanced constitutive association of βarr2. Furthermore, these receptors exhibit bias towards βarr2 recruitment over Gαi signaling pathways.

Constitutive and ligand-induced receptor internalization is enhanced in D_2R V96S/V97C mutants

β-arrestins play distinct key roles in regulating GPCR signal activity[43,44]. One function is driving receptor-mediated internalization. Given the faster (V96C) βarr2 recruitment and in particular the ligand-independent (V96S/V97C) recruitment of βarr2, the cell surface expression of these D_2Rs was assessed via flow cytometry and confocal microscopy. While all receptors were shown to traffic to the membrane (Supplementary Fig. 7), the cell surface expression of V96S/V97C was lower than WT D_2R (Fig. 4a). Due to the observation that V96S/V97C also shows increased basal βarr2 recruitment, the possibility that this decrease in cell surface expression was due to increased internalization was investigated. The percentage of constitutively internalized receptor was calculated as a percentage decrease of cell surface expression in cells incubated at 37 °C following live antibody labelling, compared to cells incubated at 4°C to prevent receptor internalization (Fig. 4b). Cells were gated to quantitate levels of D_2R in βarr2-YFP-expressing cells. An increase in constitutive internalization of V96S/V97C compared to WT receptor was observed, while Y93C had decreased internalization, and all other mutants showed comparable levels of internalization to cells expressing WT receptor. This increase in constitutive internalization may at least partially account for the decrease in cell surface expression for D_2R V96S/V97C compared to WT. There was a significant increase in ligand-induced internalization for all mutant receptors, compared to WT and this increase was most dramatic in D_2R V96S/V97C-expressing cells (Fig. 4c).

The altered ligand-induced and constitutive internalization in mutant D_2Rs observed quantitatively by flow cytometry, was also confirmed by confocal microscopy (Fig. 4d).

Transfection of lower amounts of WT D_2R plasmid resulted in lower cell-surface receptor expression and this decrease in WT expression did not cause a significant change in ligand-induced or constitutive internalization or the efficacy of quinpirole-mediated Gαi-signaling, suggesting increased internalization and decreased Gαi-signaling in receptor mutants is not solely due to lower cell surface expression (Supplementary Fig. 8c-e). Additionally, reduction in D_2R-Rluc8 WT luminescence levels to a comparable level to V96S/V97C receptor, results in the opposite effect of a decrease in basal BRET levels, suggesting that the observed increase in basal BRET associations with βarr2 in V96S/V97C-transfected cells compared to WT is not solely due to lower cell surface expression levels of mutant receptor (Supplementary Fig. 8a and b and Fig. 3). This data suggests that either faster ligand-dependent, or enhanced basal βarr2 association may promote ligand-induced internalization.

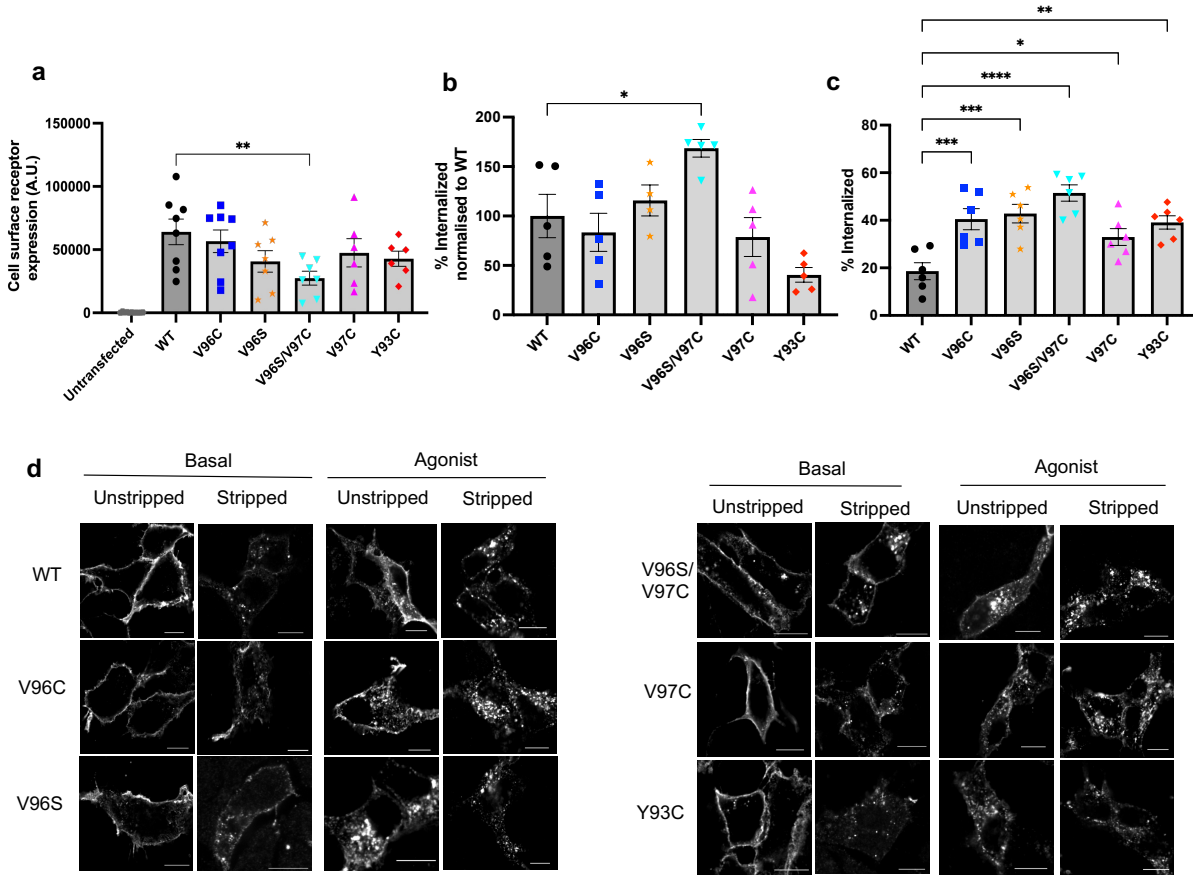

Fig. 4. Receptor cell surface expression and internalization assessed by flow cytometry and immunofluorescence microscopy. HEK293 cells transfected with D_2R constructs were labelled with M1 anti-FLAG primary and Alexa647 antibody to quantify cell surface receptor expression. (**a**) Mean fluorescence and % gated were multiplied to give a total value for cell surface D_2R expression. (**b**) In cells expressing βarr2-YFP, constitutive internalization of receptor constructs was calculated as a percentage decrease of cell surface receptor expression in cells incubated at 37°C following antibody labelling, compared to cells incubated at 4°C to prevent receptor internalization. Expressed as a percentage of WT. (**c**) Ligand-induced receptor internalization. Measured as a percentage change in cell surface expression level after ligand stimulation, compared to untreated cells. N=4-8, +/- SEM. One-way ANOVA followed by Dunnett's multiple comparison test used to measure statistical differences between WT and mutant D_2R (p*=0.0273 (b) or 0.0369 (c), p**= 0.0065 (a) or 0.0018 (c), p***<0.0009 or 0.0003, p**** <0.0001. (**d**) Representative confocal microscopy images showing D_2R localisation under basal conditions and after 30 minutes 10 μM quinpirole stimulation, with and without stripping of cell surface bound antibody. Representative of 3 independent experiments. Scale bar= 10 μm.

D_2Rs that promote βarr2 recruitment favour βarr2-mediated ERK signaling

Arrestins play well-documented roles in mediating activation of ERK signaling, therefore, the impact of these mutations on the phosphorylation levels of p44/42 extracellular signal-regulated protein kinase (ERK1/2) was assessed. D_2Rs WT, V96S and V96S/V97C increased ERK activation after quinpirole stimulation up to a maximal level after 2-5 minute stimulation (Fig. 5a-d). However, V96C exhibited enhanced agonist-dependent ERK signaling compared to WT at the 5-minute quinpirole stimulation timepoint, while V96S/V97C exhibited a more rapid ERK signaling profile (Fig. 5a and b). In CRISPR βarr1/2 knockout-cells, the ability of WT D_2R to increase phospho-ERK levels after quinpirole stimulation was maintained (Fig. 5c-e). D_2R V96C, V96S and V96S/V97C, however, exhibited a decrease in the ability to exhibit agonist-dependent ERK signaling (Fig. 5c and d). This sensitivity/requirement of βarr for ERK signaling could be due to the altered βarr2 association profiles of these D_2R mutants, which also in turn exhibit enhanced/stabilised homomer associations.

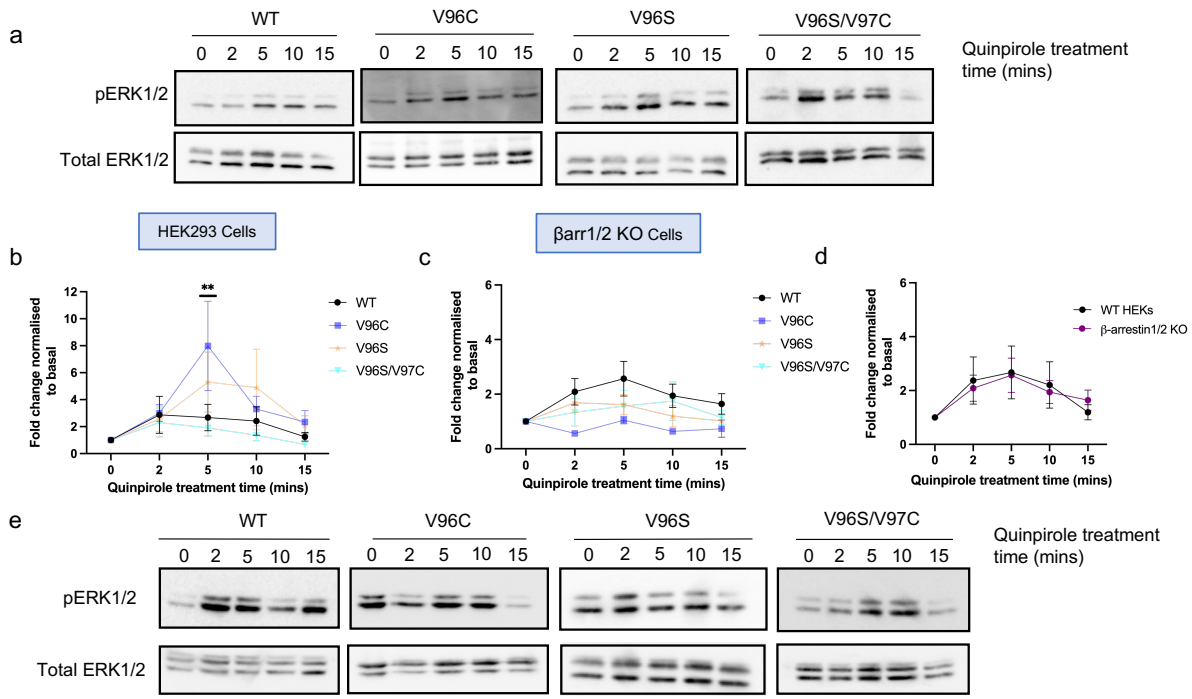

Fig. 5. Ligand induced ERK1/2 activation in HEK293 cells and βarr 1/2 knockout cells. Representative Western blots on HEK293 cells (**a** and **b**) or HEK293 βarr 1/2 KO (βarr 1/2 KO) cell lysates (**c** and **e**) transfected with D_2R constructs and treated with 10 μM quinpirole for 2, 5, 10 or 15 minutes, probed with phospho-ERK 1/2 and total ERK 1/2 antibodies. Normalised ligand-induced phospho-ERK 1/2 levels expressed as a fold change of basal levels quantified in HEK293 (**b**), or βarr 1/2 KO cell lysates (**c**) transfected with D_2R-Rluc8 WT (black) vs V96C (blue), V96S (orange), V96S/V97C (turquoise) constructs. (**d**) Direct comparison of relative pERK1/2 levels in WT HEK293 (black) or βarr 1/2 KO cells (purple) transfected with D_2R WT. Mean +/- SEM, N=3-5 for mutant receptors and N=7 for WT D_2R. Two-way ANOVA followed by Šídák's multiple comparisons test used to measure statistical differences between WT and mutant D_2R (p**<0.0052).

Modelling reveals a 2:1 D_2R:Gi and 2:2 D_2R:βarr2 stoichiometry in D_2R dimers

In order to understand how D_2R mutants and D_2R dimers may alter interactions with G-proteins and βarr2, molecular modelling was carried out. By fitting the D_2R from the cryoEM structure in complex with heterotrimeric Gi (PDB: 8IRS) onto both protomers in each of the predicted D_2R homodimers, a 2:1 D_2R:Gi stoichiometry is predicted (Supplementary Fig. 9). Steric clashes occur between two G-protein heterotrimers simultaneously docked to the D_2R homodimer, making a 2:2 stoichiometry unlikely. This suggests that the proper D_2R:Gi stoichiometry is 2:1 and any stabilisation at the H1-H2 D_2R homodimer, especially V96S/V97C, is expected to reduce the number of receptors in a conformation able to bind to heterotrimeric Gi, thus reducing coupling efficiency.

Docking simulations between the homodimers of D_2R WT, V96C, and V96S/V97C and two different structural models of βarr2 always predicted receptor-arrestin complexes similar to the cryoEM complexes (see Methods). It is worth noting that in all dimeric complexes, the D_2R is in an active state as it was extracted from the cryoEM complex the agonist ritigotine and heterotrimeric Gi (PDB: 8IRS). Remarkably, the architecture of the H1-H2 D_2R dimers favors the simultaneous recruitment of two βarr2 molecules (i.e. with a D_2R:βarr2 2:2 stoichiometry) (Fig. 6a and b). Noticeably, the finger loop holds a different conformation in the two βarr2 models, which was inherited from the two different βarr1 structural templates, the finger loop being unstructured in 6TKO while holding one α-helical turn in 7SRS. In the predicted complexes between WT or mutant D_2R dimers and both βarr2 structural models, the finger loop of βarr2 docks in the receptor site contributed by cytosolic extensions of H3 and H6 as well as ICL1, ICL2, and H8. Furthermore, the middle loop and the β-hairpin that includes the

C-loop of βarr2 make contacts with ICL2 of the receptor (Fig. 6a and b). While the interface described above is common to all prototypical GPCRs, an additional interface between the N-terminal domain of βarr2 and the phosphorylated tail of the receptor is formed only when such tail is present, which is not the case of D_2R.[45] Lack of the phosphorylated C-tail may have an effect on the process of βarr-receptor recognition but not on the final architecture of the complex, which is expected to be the same independently of presence or absence of the C-tail. Therefore, the D_2R dimer-stabilising mutants both reduce the number of receptors available for Gαi coupling, whilst favoring βarr2 coupling. BRET saturation assays in βarr 1/2 KO cells suggested that βarr 1/2 was not required for D_2R dimerization, but an increase in ligand-induced BRETmax was observed in D_2R WT expressing βarr 1/2 KO cells compared to WT HEK293 cells (Supplementary Fig. 1e-h). This may suggest that D_2R dimers form distinct conformations in the presence or absence of βarrs.

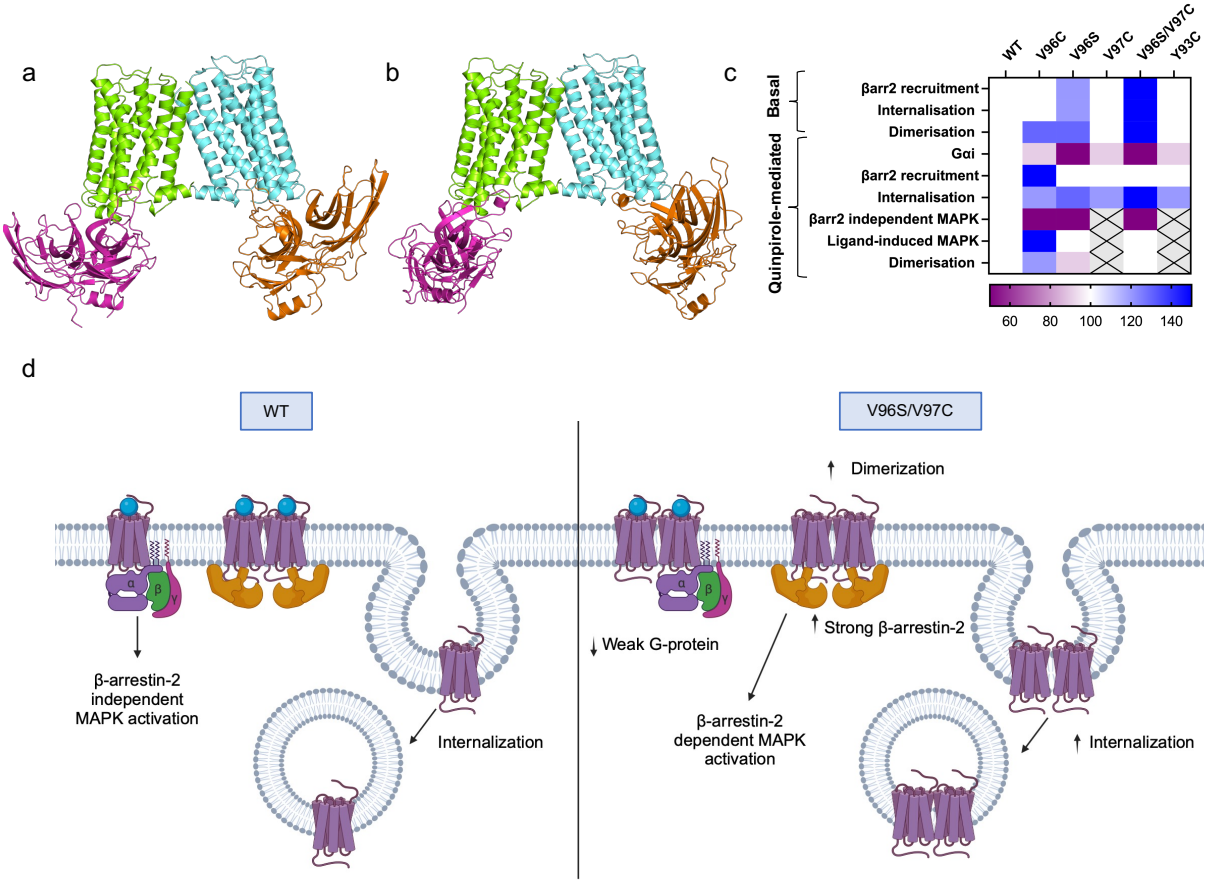

Fig. 6. Predicted models for D_2R homodimer-βarr2 complexes and summary schematics. The cartoon representations of two different structural complexes between the V96S/V97C mutant D_2R homodimer (protomers lemon-green and aquamarine) and βarr2 (structures orange and magenta) are shown. The structural models of βarr2 shown in the **a** and **b** panels have been, respectively, achieved by using the βarr1 structures from the 6TKO and 7SRS cryoEM complexes as templates. (**c**) Heat map summarising the functional effects of D_2R mutants relative to WT where 100 is WT and white, an increase relative to WT is blue and a decrease is purple. (**d**) Summary schematic of proposed βarr2 biased signaling from D_2R V96S/V97C oligomers.

Discussion

Combining molecular docking simulations with biophysical, super-resolution and functional studies, we propose a model for stabilising D_2R homomer associations, and demonstrate the utility of such an approach to identify a mechanism for not only stabilising receptor-receptor associations, but also for promoting βarr2 interaction and βarr2-mediated functions. This reveals a potential role for D_2R di/oligomerization in βarr2-biased signaling that could be targeted for therapeutic benefits.

The D_2R homomer interface characterised by H1-H1, H1-H2, H2-H2 contacts is shared with other published high-resolution GPCR dimer structures including rhodopsin, κ-opioid, β1-adrenergic, μ-opioid, and human apelin receptors[46–50]. Previous studies have suggested that H4 participates in D_2R homodimer interface, but a second interface involving H1 and H8 has also been suggested[29,51,52]. Additionally, several studies have suggested that ICL1, ECL2 and ECL3 are important in stabilising GPCR dimer interactions[52–54]. However, this is based on computational modelling and biophysical data, with no current published dimer structure for the D_2R homodimer. It is also possible that multiple dimer interfaces exist, as reported for the β1AR, where both a H1-H2-H8-ECL1 and H4-H5-ECL2-ICL2 interfaces exist[46]. Given we observed both dimers and higher-order oligomers, we cannot rule out that D_2R interacts through additional interfaces depending on whether it exists in a dimeric or higher-order complex. Mutations at specific sites of the interface predicted herein increased the stability of D_2R homomers, with the V96S/V97C double mutant exhibiting the greatest shift towards D_2Rs in an oligomeric state in the absence of ligand (~6% increase), indicating an increase in constitutive oligomer stability. Super-resolution, single molecule analysis revealed there was little change in the proportion of WT and

V96S/V97C D_2Rs in an oligomeric state after cells were stimulated with quinpirole. Interestingly, the proportion of V96S receptors in an oligomeric complex at the cell surface were reduced when stimulated with quinpirole, which could reflect that di/oligomers of this D_2R are internalized, which is consistent with the enhanced ligand-induced internalization and oligomerization favouring βarr2 coupling.

Ligand bias, whereby ligands can promote one pathway over another, are of interest both therapeutically and for understanding the molecular basis of pathway preferences for different GPCRs, in different conformational states[55,56]. In this study, receptor mutants, which showed increased di/oligomerization also showed increased ligand induced (V96C and V96S) or constitutive (V96S/V97C) associations with βarr2 (Summarised in Fig. 6c and d). There are many factors that can affect the signaling pathway preference of a GPCR, including membrane lipid composition and localisation of receptors[36,57–60]. Interestingly, these factors have also been shown to influence oligomerization of GPCRs[61]. While changes in the organisation of D_2R complexes at the cell surface detected in PD-PALM experiments may be small, even slight changes in complex formation can have dramatic effects on receptor signaling in cells[38,39]. By enhancing specific receptor conformations such as a propensity to oligomerise and associate with βarr2, the role of such conformations on receptor activity may be amplified. There is some debate about the role of βarrs in D_2R-mediated ERK activation. It is likely that mechanisms are cell-type specific and D_2R isoform specific, with D_2R long and short differing in the way they mediate MAPK activation[62,63]. Interestingly, the apparent bias towards βarr2 recruitment in D_2R mutants results in a βarr2-dependent mechanism for downstream mediation of the MAPK pathway. However, this does not seem to be the case for WT D_2R, with ERK activation

maintained in βarr1/2 KO cells (Fig. 5e-h). Additionally, these mutants exhibit increased quinpirole-induced internalization, with the V96S/V97C mutant also showing increased constitutive internalization (Fig. 4b and c). It is possible that increased dimerization of these mutants makes them more likely to internalise as has been demonstrated from CXCR4 oligomers[20]. Taken together, the most striking changes in signaling under basal conditions are observed with the D_2R V96S/V97C double mutation, which causes changes in D_2R conformation to show a strong preference for βarr2, which is required for downstream signaling.

Most current work on the impact of oligomerization on biased signaling has been done on heteromers rather than homomers, including the $A_{2A}R$-D_2R heteromer[64,65]. Previous studies on the impact of GPCR dimerization on G-protein activation have found that oligomerization can either increase or decrease G-protein activation, suggesting there is no consensus for all GPCRs in one class, but such behaviour is receptor specific[20,22,66,67]. The role of oligomerization on βarr recruitment has been less well studied. Oligomerization of the PAFR has been shown to cause a bias away from βarr recruitment, while our study shows the opposite trends for the D_2R[22] .It has been suggested that allosteric interactions between receptor protomers upon receptor activation of the $A_{2A}R$-D_2R heteromer, causes the D_2R protomer to favour βarr2 recruitment[65]. It is possible that a similar phenomenon is occurring in the D_2R mutant homomers explored in this study which show increased βarr2 recruitment and associated signaling, with an increase in D_2R homomer stability.

Dimerization has been suggested to significantly increase the surface area available for arrestins to bind, which may provide a rationale for the increased oligomerization,

which we observe in receptor mutants that also show a bias towards arrestin-mediated signaling pathways[12,68]. It is possible that the V96S/V97C double mutant and, to some extent, the V96S D_2R mutant, are showing a more 'active-like' conformation in the absence of agonists, which causes them to associate more readily with βarr2, causing increased internalization and a dependence upon βarr2 for MAPK signaling. Previous studies have found that βarrs are involved in D_2R-mediated ERK phosphorylation in the $A_{2A}R$-D_2R heteromer, but not when D_2R is expressed alone[69]. It is also possible that for these D_2R mutants, increased homo-oligomerization induces increased dependence upon βarr2 for signaling pathways. This is supported by docking simulations between D_2R homodimers and βarr2, which showed a 2:2 receptor: βarr2 stoichiometry while showing a 2:1 receptor: Gi stoichiometry (Fig. 6a and b and Supplementary Fig. 9). This suggests that D_2R dimers, and therefore mutations which stabilise homo-di/oligomers, favour βarr2 coupling over Gi coupling. These docking simulations may provide an insight into the structural basis behind the observed increase in oligomerization in D_2R mutants that also exhibit increased βarr2 associations.

In conclusion, the role of D_2R oligomers in disease makes these complexes attractive therapeutic targets[31,70–72]. The lack of high-resolution structures of the D_2R homodimer has hindered our ability to exploit oligomers for therapeutic benefits. Here we suggest models for the D_2R homodimer and experimental validation confirms a key role for H2 at the predicted D_2R homodimer interface to increase dimer stability, and a bias towards βarr2. These mutant constructs could form the basis for structural studies capturing D_2R homomers and specific D_2R- βarr complexes. More broadly, this study provides a framework for engineering the stabilisation of class A GPCR dimers and

may suggest that D_2R oligomers favour an ‘active-like’ conformation that promotes βarr recruitment.

Methods

Molecular modelling

Prediction of likely architectures of D_2R homodimers relied on a computational approach developed for quaternary structure predictions of transmembrane α-helical proteins, including a number of GPCRs, i.e. FiPD-based approach[73–75]. It consists of rigid-body docking using both a version of the ZDOCK program devoid of desolvation as a component of the docking score (v2.1)[76] , followed by employment of a membrane topology filter by the FiPD software to minimize false positives and allow cluster analysis for selecting the final solutions. Both inactive- and active-state D_2R homodimers were predicted. In this respect, the 6CM4 structure completed with the missing IL2 was used as an inactive state, whereas the receptor structure extracted from the cryoEM complex with rotigotine and heterotrimeric miniGi (PDB: 8IRS) was used as an active state. The employment of an active-state structural model of D_2R was instrumental in predicting supramolecular complexes between D_2R dimers and either βarr1 or βarr2. The latter predictions were also carried out by ZDOCK v3.0.2[77] coupled with a FiPD-based filtering approach based on a distance cutoff between the DRY arginine (R132) of D_2R and L/V71 in the finger loops of βarr1 or βarr2, respectively, followed by cluster analysis. In those docking simulations, the receptor was used as a fixed target while βarr1 or βarr2 was used as a probe. The structural model of receptor-bound βarr2 were achieved by comparative modelling (by Modeller[78]), using the cyoEM structures of βarr1 bound either to the β_1-AR (PDB: 6TKO) or to the $5HT_{2B}$ receptor (PDB: 7SRS) as templates. Remarkably, the two βarr1 templates differed in the conformation of several loops including the finger loop, an essential recognition point for receptor binding. Such comparative modelling was necessary because none of the available βarr2 structures, co-crystallized with

peptides from the C-tails of a number of GPCRs, represent real receptor-bound forms as far as conformation and arrangements of the loops in the central crest are concerned. Accordingly, the employment of those βarr2 structures in docking simulations with the D_2R did not produce any reliable solution. The employment of two different structural models of βarr2 served to overcome in part the lack of cryoEM complexes of βarr2 with GPCRs and to take into account possible structural variability in the receptor-bound states of the same arrestin. For βarr1, the most complete versions of the cryoEM structures 6TKO and 7SRS were employed. Only the results of βarr2-D_2R docking are shown here. Evaluation of the native-like feature of a docking solution was based on structural comparisons with the cryoEM receptor-βarr1 complexes (6TKO and 7SRS).

Cell Culture and transfection

HEK293 cells (human embryonic kidney cells) and βarr1/2 knockout cells were maintained as a monolayer in T-75 cm2 flasks (Sigma). βarr1/2 knockout HEK293 cells were made by using CRISPR-Cas9 (kindly provided by Asuka Inoue, Univ. Tohoku). Cells were cultured in Dulbecco's Modified Eagle's Medium (DMEM) media (Gibco) containing 4.5 g/L glucose, 1% (v/v) L-glutamine and supplemented with 10% (v/v) FBS (Gibco), 1% (v/v) streptomycin/penicillin (Sigma) in a humidified atmosphere of 5% CO_2 at 37°C. Cells were usually passaged every 3-4 days in a 1:10 ratio using 0.05% (v/v) trypsin (Gibco, UK) in phosphate buffered saline (PBS). HEK293 cells were seeded and cultured in 6 well plates 1 day before transfection in DMEM with 10% (v/v) FBS (Gibco), 1% (v/v) streptomycin/penicillin (Sigma). Cells were transfected at 80-90% confluency with Lipofectamine 2000 reagent (Invitrogen, UK).

Plasmid DNA constructs

βarr1-YFP and βarr2-YFP plasmids were obtained from Frederic Jean-Alphonse (CNRS, Nouzilly). FLAG-D_2R-Venus and Rluc8 plasmids were obtained from Jonathan Javitch. The FLAG-D_2R-Rluc8 plasmid was used to obtain the D_2R Cys mutant constructs using the Agilent Quikchange II site-directed Mutagenesis Kit according to the manufacturer's instructions. Mutant D_2R constructs were introduced into D_2R-Venus plasmids via the In-Fusion Snap Assembly cloning kit (Takara) according to manufactures instructions and inserted into FLAG-D_2R-Venus DNA using BamHI and Kpn1 restriction sites.

BRET saturation assays

Cells were transfected with constant amounts of D_2R-Rluc8 plasmid DNA and increasing amounts of D_2R-Venus (0-3 µg in 6 well plates) plasmid and assayed 48 hours post-transfection. Cells in suspension were plated in white 96 well plates in triplicate. Coelenterazine-h (Promega) was used at a final concentration of 5 µM. BRET emissions using the short-wavelength filter at 475 nm and long wavelength filter 535 nm were measured in 10 repeat cycles using a LUMIstarOPTIMA plate reader (BMG Labtech). Fluorescence of Venus-tagged receptor was measured in duplicate after excitation at 485 nm and emission at 535 nm.

For each condition, net BRET values were calculated (535 nm value/ 475 nm value) over 10 cycles, where BRET ratios for the negative control donor only condition were subtracted. Rluc8 values (475 nm emission value) were averaged over the 10 cycles and again for the duplicate repeats. Net Venus values were calculated by subtracting Venus measurements of donor only conditions. Net BRET values were plotted against

Net Venus/Rluc8 using GraphPad Prism 10 and fitted with a non-linear binding curve assuming one site-specific binding.

β-arr recruitment BRET assays

HEK293 cells were transfected with D_2R-Rluc8 plasmids and βarr1/2-YFP constructs. 48 hours post transfection cells were resuspended in PBS. For BRET time course assays, Venus expression (excitation 485 and emission 535 nm) was measured. For basal BRET emissions, a separate set of duplicate cell suspensions were measured at 475 nm excitation and 535 nm emission wavelengths after addition of 5 μM coelenterazine-h (Promega). PBS or 10 μM quinpirole was added to cell suspensions and BRET emissions were immediately measured again. Raw BRET ratios were calculated (535 nm value/ 475 nm value). To calculate ligand induced BRET, basal BRET ratios were subtracted from BRET ratios after agonist addition. For dose response BRET experiments, increasing concentrations of quinpirole agonist was added to sets of duplicate cell suspensions after basal BRET emissions had been measured. After ligand induced BRET values had been calculated, data was normalised by subtracting the control with only PBS added.

Analysis was based on βarr recruitment waveform methods as previously described [79]. The BRET emissions were measured every 3-5 seconds for a total of 5 minutes. Ligand-induced BRET ratios were calculated and plotted against time and recruitment of βarr was observed to be stable recruitment, where the waveform rises to a steady state. The waveforms were fitted to non-linear one-phase association curve in GraphPad Prism 10 to allow quantification of kinetics. The rate constant s-1 was quantified and can be represented as the halftime, in seconds, (computed as ln(2)/k).

The steady-state level of recruitment is represented as the plateau of the waveform, which also indicates the affinity of the receptor for βarr. The initial rate of recruitment was also calculated as k*span (maximum BRET ratio).

Flow cytometry

Cells were live labelled with M1 anti-FLAG antibody (1:1000 Sigma Aldrich, no.3040) 48 hours post transfection for 30 minutes at 37 °C. For the flow internalization assay, antibody incubation was carried out at 4°C for 1 hour for all cells, then one set of cells were transferred to the 37 °C incubator and allowed to recover for 1 hour. Agonist stimulation at 37°C was carried out 30 minutes in to the 1-hour recovery period. The other set of cells was kept at 4 °C and washed 3 times with cold DMEM media. Cells were resuspended in FACS buffer (PBS with $Ca^{2+}$and Mg^{2+} and 2% FBS), centrifuged and the cells resuspended in either FACS buffer alone for untreated cells or with Alexa Fluor 647 antibody (1:2000; Invitrogen, A32728). Cell suspensions were incubated for 1 hour on ice and washed in FACS buffer three times. The cell suspensions were transferred to individual round bottomed polypropylene tubes and the immunofluorescence measured on a FACS Calibur Flow Cytometer (BD biosciences).

cAMP assay

HEK293 were transfected with 1 µg of D_2R-Rluc8 constructs. After 24 hours, approximately 40,000 cells/well were replated into a 96-well format in triplicate for each condition. After a further 24 hours, the cells washed with PBS and pre-treated with 0.5 mM IBMX in DMEM with 0.1% Bovine serum albumin (BSA) for 5 minutes at 37°C. Forskolin was diluted in 0.5mM IMBX in DMEM 0.1% BSA to give a final concentration of 3 µM. Cells were stimulated with ligands diluted in the forskolin solution and incubated at 37°C. After stimulation, cells were washed with ice cold PBS and lysed. The level of cAMP in lysates was measured using the cAMP Gs Dynamic 2 kit (Revvity).

Western blotting

Cells were washed with PBS and lysed with ice cold RIPA lysis buffer (50 mM Tris pH7.4, 1% Triton X-100, 140 mM NaCl, 5 mM EDTA, 1 mM NaF, 1 mM PMSF, 1 mM sodium orthovandate and a protease inhibitor tablet (Roche)). Protein concentrations were determined using BSA standard curve and diluted in Laemmli sample buffer (Sigma) in the presence or absence of 5% 2-β-mercaptoethanol. Samples were separated via SDS-polyacrylamide gel and transferred to a nitrocellulose membrane. The membrane was blocked and incubated in primary antibody diluted overnight (See Supplementary Table 1). Membranes were incubated in HRP-linked secondary antibody and imaged using Immobilon Forte Western HRP reagent (Millipore) and X-ray film (Amersham) or Chemi-imager. The band intensities were analysed using Image J.

For pERK Western blotting, cells were serum starved for 16 hours before quinpirole stimulation and lysis of cells. All lysates were diluted to 20 µg of protein in Laemmli buffer in the presence of 5% 2-β-mercaptoethanol, boiled for 5 minutes at 95°C before loading. Quantification of protein intensity was done separately for each blot and where multiple blots were used the same D_2R WT lysates were employed to allow direct comparison with mutant D_2R on the same membrane.

Confocal Microscopy

Transfected cells were replated onto coverslips in a 24 well format with approximately 75,000 cells/well and left for a further 24-48 hours. Cells were incubated in M1 anti-FLAG antibody (Sigma Aldrich, no.3040) diluted 1:500 with or without 10 µM quinpirole for 30 minutes at 37°C. To remove the cell surface antibody, cells were washed 3 times with 0.04 M EDTA in PBS-Ca^{2+} before fixation. Cells were then fixed with 4% PFA in PBS-Ca^{2+}, permeabilised with 0.2% Triton-X in PBS-Ca^{2+} and blocked for 1 hour at RT in 2% FBS in PBS-Ca^{2+}prior to incubation in Alexa Fluro-conjugated secondary antibody (1:000 dilution) (Thermofisher, A32728). Slides were mounted onto coverslips and imaged were obtained with a Leica Stellaris 8 microscope using a 64 x oil immersion objective and sequential excitation at wavelengths of 405, 488 and 647 nm.

PD-PALM

Transfected cells were plated onto 35mm dishes (Mattek) with 14mm x 1.5mm glass coverslips. Anti-FLAG (Sigma Aldrich) primary antibodies were labelled with photo switchable dye CAGE 500 according to the manufacturer's instructions (Abberior). Live cells were incubated with FLAG-CAGE500 conjugated antibody, diluted in 10% FCS in PBS Ca2+, at 37 °C for 30 minutes. All steps from antibody addition to imaging were carried out in the dark to prevent activation on the conjugated antibodies. Cells were washed in PBS Ca2+ before fixation in 4% PFA and 0.2% Glutaraldehyde for 30 minutes (Sigma) and maintained in PBS Ca^{2+}.

PALM images were acquired using the Zeiss Eyra PS1 microscope with 1.45 numerical aperture, 100x oil immersion objective in total internal reflection fluorescence (TIRF) mode. Photoactivation of CAGE 500 dye was achieved by simultaneous activation with 405 nm (UV light) and excitation and photobleaching with 488 nm laser. Lasers were switched on 30 minutes before imaging to allow stabilisation. Images were captured over 20,000 frames with an exposure time of 100 ms using the ZEN software.

Location analysis of receptors was done using the QuickPALM plugin in Fiji, as previously described [80]. Two 7x7 μM region of interests were analysed within the cell boundary using the QuickPALM plugin. The parameters used were typically a signal to noise ratio of 7 and a full-half width maximum of 5, although these were determined for each experiment. This analysis outputs XY coordinates of the localised particles with sub-pixel accuracy. Particles within 20 nm of each other were discounted to prevent overestimation of receptor complexes. The coordinates were inputted into a

Java- based PD-interpreter application [39,40]. to determine the number of associated receptor molecules. This app uses Getis-Franklin neighbourhood analysis with a search radius of 50 nm. The software discounts a receptor from further searches once it has been assigned as participating in a homomer, to prevent double counting. The output is a table containing both the number of associations and the number of receptor molecules in each complex.

Quantification and statistical analysis

All statistical analysis was performed in GraphPad Prism 10. Specific statistical tests are noted in each figure legend. In most cases, two-tailed, unpaired t-tests was used when comparing two groups or one-way ANOVA with Dunnett's multiple comparison test was used for multiple groups. For comparing two variables and multiple groups, two-way ANOVA followed by Šídák's multiple comparisons test was used. In all tests, $p<0.05$ was considered statistically significant.

References

1. Syrovatkina, V., Alegre, K. O., Dey, R. & Huang, X.-Y. Regulation, Signaling, and Physiological Functions of G-Proteins. *J Mol Biol* **428**, 3850–3868 (2016).
2. Hauser, A. S., Attwood, M. M., Rask-Andersen, M., Schiöth, H. B. & Gloriam, D. E. Trends in GPCR drug discovery: new agents, targets and indications. *Nat Rev Drug Discov* **16**, 829–842 (2017).
3. Yang, D. *et al.* G protein-coupled receptors: structure- and function-based drug discovery. *Signal Transduct Target Ther* **6**, 7 (2021).
4. Wootten, D., Christopoulos, A., Marti-Solano, M., Babu, M. M. & Sexton, P. M. Mechanisms of signaling and biased agonism in G protein-coupled receptors. *Nat Rev Mol Cell Biol* **19**, 638–653 (2018).
5. Shenoy, S. K. & Lefkowitz, R. J. β-arrestin-mediated receptor trafficking and signal transduction. *Trends Pharmacol Sci* **32**, 521–533 (2011).
6. Pin, J.-P. *et al.* International Union of Basic and Clinical Pharmacology. LXVII. Recommendations for the Recognition and Nomenclature of G Protein-Coupled Receptor Heteromultimers. *Pharmacol Rev* **59**, 5 LP – 13 (2007).
7. Ferré, S. *et al.* G protein-coupled receptor-effector macromolecular membrane assemblies (GEMMAs). *Pharmacol Ther* **231**, 107977 (2022).
8. Angers, S. *et al.* Detection of β2-adrenergic receptor dimerization in living cells using bioluminescence resonance energy transfer (BRET). *Proceedings of the National Academy of Sciences* **97**, 3684–3689 (2000).
9. Motterlini, R. & Otterbein, L. E. The therapeutic potential of carbon monoxide. *Nature Reviews Drug Discovery* **9** 728–743 (2010).
10. Whorton, M. R. *et al.* A monomeric G protein-coupled receptor isolated in a high-density lipoprotein particle efficiently activates its G protein. *Proceedings of the National Academy of Sciences* **104**, 7682–7687 (2007).
11. Asher, W. B. *et al.* Single-molecule FRET imaging of GPCR dimers in living cells. *Nat Methods* **18**, 397–405 (2021).
12. Ferré, S. *et al.* G protein-coupled receptor oligomerization revisited: Functional and pharmacological perspectives. *Pharmacological Reviews* **66**, 413–434 (2014).
13. Ferré, S. *et al.* Building a new conceptual framework for receptor heteromers. *Nature Chemical Biology,* **5***,* 131–134*.* (2009).
14. Kasai, R. S. & Kusumi, A. Single-molecule imaging revealed dynamic GPCR dimerization. *Curr Opin Cell Biol* **27**, 78–86 (2014).
15. Tabor, A. *et al.* Visualization and ligand-induced modulation of dopamine receptor dimerization at the single molecule level. *Sci Rep* **6***,* 33233 (2016).
16. Calebiro, D. *et al.* Single-molecule analysis of fluorescently labeled G-protein–coupled receptors reveals complexes with distinct dynamics and organization. *Proceedings of the National Academy of Sciences* **110**, 743–748 (2013).
17. Hern, J. A. *et al.* Formation and dissociation of M1 muscarinic receptor dimers seen by total internal reflection fluorescence imaging of single molecules. *Proceedings of the National Academy of Sciences* **107**, 2693–2698 (2010).
18. Milligan, G. The role of dimerisation in the cellular trafficking of G-protein-coupled receptors. *Curr Opin Pharmacol* **10**, 23–29 (2010).
19. Ferre, S., Von Euler, G., Johansson, B., Fredholm, B. B. & Fuxe, K. Stimulation of high-affinity adenosine A2 receptors decreases the affinity of dopamine D2 receptors in rat striatal membranes. *Proc Natl Acad Sci U S A* **88,** 7238–7241 (1991).

20. Ge, B. *et al.* Single-molecule imaging reveals dimerization/oligomerization of CXCR4 on plasma membrane closely related to its function. *Sci Rep* **7**, 16873 (2017).
21. Rodríguez-Frade, J. M., Mellado, M. & Martínez-A, C. Chemokine receptor dimerization: two are better than one. *Trends Immunol* **22**, 612–617 (2001).
22. Liu, J. *et al.* Biased signaling due to oligomerization of the G protein-coupled platelet-activating factor receptor. *Nat Commun* **13**, 6365 (2022).
23. Sun, Y. *et al.* Single-molecule imaging reveals the stoichiometry change of β2-adrenergic receptors by a pharmacological biased ligand. *Chem. Commun.* **52**, 7086–7089 (2016).
24. Gusach, A., García-Nafría, J. & Tate, C. G. New insights into GPCR coupling and dimerisation from cryo-EM structures. *Curr Opin Struct Biol* **80**, 102574 (2023).
25. Neve, K. A., Seamans, J. K. & Trantham-Davidson, H. Dopamine Receptor Signaling. *J Recept Signal Transduct Res* **24***,* 165–205 (2004).
26. Missale, C., NASH, S. R., ROBINSON, S. W., JABER, M. & CARON, M. G. Dopamine Receptors: From Structure to Function. *Physiol Rev* **78**, 189–225 (1998).
27. Beaulieu, J.-M. & Gainetdinov, R. R. The Physiology, Signaling, and Pharmacology of Dopamine Receptors. *Pharmacol Rev* **63**, 182 LP – 217 (2011).
28. Albizu, L. *et al.* Time-resolved FRET between GPCR ligands reveals oligomers in native tissues. *Nat Chem Biol* **6**, 587–594 (2010).
29. Guo, W. *et al.* Dopamine D2 receptors form higher order oligomers at physiological expression levels. *EMBO Journal* **27**, 2293-304 (2008).
30. Kasai, R. S., Ito, S. V, Awane, R. M., Fujiwara, T. K. & Kusumi, A. The Class-A GPCR Dopamine D2 Receptor Forms Transient Dimers Stabilized by Agonists: Detection by Single-Molecule Tracking. *Cell Biochem Biophys* **76**, 29–37 (2018).
31. Wang, M. *et al.* Schizophrenia, amphetamine-induced sensitized state and acute amphetamine exposure all show a common alteration: increased dopamine D2 receptor dimerization. *Mol Brain* **3**, 25 (2010).
32. Masri, B. *et al.* Antagonism of dopamine D2 receptor/β-arrestin 2 interaction is a common property of clinically effective antipsychotics. *Proc Natl Acad Sci U S A* **105**, 13656–13661 (2008).
33. Wang, S. *et al.* Structure of the D2 dopamine receptor bound to the atypical antipsychotic drug risperidone. *Nature* **555**, 269 (2018).
34. Fan, L. *et al.* Haloperidol bound D2 dopamine receptor structure inspired the discovery of subtype selective ligands. *Nat Commun* **11**, 1074 (2020).
35. Yin, J. *et al.* Structure of a D2 dopamine receptor-G-protein complex in a lipid membrane. *Nature* **584**, 125 (2020).
36. Buenaventura, T. *et al.* Agonist-induced membrane nanodomain clustering drives GLP-1 receptor responses in pancreatic beta cells. *PLoS Biol* **17**, e3000097 (2019).
37. Casarini, L. *et al.* Membrane Estrogen Receptor (GPER) and Follicle-Stimulating Hormone Receptor (FSHR) Heteromeric Complexes Promote Human Ovarian Follicle Survival. *iScience* **23**, (2020).
38. Walker, A. R. *et al.* Functional rewiring of G protein-coupled receptor signaling in human labor. *Cell Rep* **40**, (2022).
39. Jonas, K. C. *et al.* Temporal reprogramming of calcium signaling via crosstalk of gonadotrophin receptors that associate as functionally asymmetric heteromers. *Sci Rep* **8**, 2239 (2018).
40. Jonas, K. C., Fanelli, F., Huhtaniemi, I. T. & Hanyaloglu, A. C. Single Molecule Analysis of Functionally Asymmetric G Protein-coupled Receptor (GPCR) Oligomers

Reveals Diverse Spatial and Structural Assemblies. *Journal of Biological Chemistry* **290**, 3875–3892 (2015).
41. Beaulieu, J. M. *et al.* An Akt/β-arrestin 2/PP2A signaling complex mediates dopaminergic neurotransmission and behavior. *Cell* **122**, 261 (2005).
42. Skinbjerg, M. *et al.* Arrestin3 mediates D2 dopamine receptor internalization. *Synapse* **63**, 621–624 (2009).
43. Shukla, A. K., Xiao, K. & Lefkowitz, R. J. Emerging paradigms of β-arrestin-dependent seven transmembrane receptor signaling. *Trends Biochem Sci* **36**, 457–469 (2011).
44. DeWire, S. M., Ahn, S., Lefkowitz, R. J. & Shenoy, S. K. β-Arrestins and Cell Signaling. *Annu Rev Physiol* **69**, 483–510 (2007).
45. Maharana, J. *et al.* Structural snapshots uncover a key phosphorylation motif in GPCRs driving β -arrestin activation. *Mol Cell* **83**, 2091-2107.e7 (2023).
46. Huang, J., Chen, S., Zhang, J. J. & Huang, X. Y. Crystal structure of oligomeric β 1-adrenergic G protein-coupled receptors in ligand-free basal state. *Nat Struct Mol Biol* **20**, 419–425 (2013).
47. Salom, D. *et al.* Crystal structure of a photoactivated deprotonated intermediate of rhodopsin. *Proceedings of the National Academy of Sciences* **103**, 16123 LP – 16128 (2006).
48. Manglik, A. *et al.* Crystal structure of the μ-opioid receptor bound to a morphinan antagonist. *Nature* **485**, 321–326 (2012).
49. Wu, H. *et al.* Structure of the human κ-opioid receptor in complex with JDTic. *Nature* **485**, 327–332 (2012)
50. Yue, Y. *et al.* Structural insight into apelin receptor-G protein stoichiometry. *Nat Struct Mol Biol* **29**, 688–697 (2022).
51. Guo, W., Shi, L. & Javitch, J. A. The fourth transmembrane segment forms the interface of the dopamine D2 receptor homodimer. *Journal of Biological Chemistry* **278**, 4385–4388 (2003).
52. Bueschbell, B. *et al.* The World of GPCR dimers: Mapping dopamine receptor D_2 homodimers in different activation states and configuration arrangements. *Comput Struct Biotechnol J* **21**, 4336–4353 (2023).
53. Johnston, J. M. *et al.* Making Structural Sense of Dimerization Interfaces of Delta Opioid Receptor Homodimers. *Biochemistry* **50**, 1682–1690 (2011).
54. Pulido, D. *et al.* Design of a True Bivalent Ligand with Picomolar Binding Affinity for a G Protein-Coupled Receptor Homodimer. *J Med Chem* **61**, 9335–9346 (2018).
55. Lane, J. R., May, L. T., Parton, R. G., Sexton, P. M. & Christopoulos, A. A kinetic view of GPCR allostery and biased agonism. *Nat Chem Biol* **13**, 929–937 (2017).
56. Seyedabadi, M., Ghahremani, M. H. & Albert, P. R. Biased signaling of G protein coupled receptors (GPCRs): Molecular determinants of GPCR/transducer selectivity and therapeutic potential. *Pharmacol Ther* **200**, 148–178 (2019).
57. Damian, M. *et al.* Allosteric modulation of ghrelin receptor signaling by lipids. *Nat Commun* **12**, 3938 (2021).
58. Dawaliby, R. *et al.* Allosteric regulation of G protein–coupled receptor activity by phospholipids. *Nat Chem Biol* **12**, 35–39 (2016).
59. Hanson, M. A. *et al.* A Specific Cholesterol Binding Site Is Established by the 2.8 Structure of the Human & β 2-Adrenergic Receptor. *Structure* **16**, 897–905 (2008).
60. Kockelkoren, G. *et al.* Molecular mechanism of GPCR spatial organization at the plasma membrane. *Nat Chem Biol* **20**, 142–150 (2023).

61. Gahbauer, S. & Böckmann, R. A. Membrane-Mediated Oligomerization of G Protein Coupled Receptors and Its Implications for GPCR Function. *Frontiers in Physiology* **7**, 494 (2016).
62. Quan, W., Kim, J.-H., Albert, P. R., Choi, H. & Kim, K.-M. Roles of G protein and β-arrestin in dopamine D2 receptor-mediated ERK activation. *Biochem Biophys Res Commun* **377**, 705–709 (2008).
63. Kim, S. J., Kim, M. Y., Lee, E. J., Ahn, Y. S. & Baik, J. H. Distinct regulation of internalization and mitogen-activated protein kinase activation by two isoforms of the dopamine D2 receptor. *Molecular Endocrinology* **3**, 640–652 (2004).
64. Mores, K. L., Cassell, R. J. & van Rijn, R. M. Arrestin recruitment and signaling by G protein-coupled receptor heteromers. *Neuropharmacology* **152**, 15–21 (2019).
65. Borroto-Escuela, D. O. *et al.* On the existence of a possible A2A-D2-β- arrestin2 complex: A2A agonist modulation of D2 agonist-induced β-arrestin2 recruitment. *J Mol Biol* **406**, 687-99 (2011).
66. White, J. F. *et al.* Dimerization of the class A G protein-coupled neurotensin receptor NTS1 alters G protein interaction. *Proceedings of the National Academy of Sciences* **104**, 12199–12204 (2007).
67. Arcemisbéhère, L. *et al.* Leukotriene BLT2 Receptor Monomers Activate the G_{i2} GTP-binding Protein More Efficiently than Dimers . *Journal of Biological Chemistry* **285**, 6337–6347 (2010).
68. Maurice, P., Kamal, M. & Jockers, R. Asymmetry of GPCR oligomers supports their functional relevance. *Trends Pharmacol Sci* **32**, 514–520 (2011).
69. Huang, L., Wu, D., Zhang, L. & Feng, L. Modulation of A2a receptor antagonist on D2 receptor internalization and ERK phosphorylation. *Acta Pharmacol Sin* **34**, 1292–1300 (2013).
70. Bonaventura, J. *et al.* Allosteric interactions between agonists and antagonists within the adenosine A2a; receptor-dopamine D2 receptor heterotetramer. *Proceedings of the National Academy of Sciences* **112**, E3609 LP-E3618 (2015).
71. Fuxe, K. *et al.* Adenosine-dopamine interactions in the pathophysiology and treatment of cns disorders. *CNS Neuroscience and Therapeutics* Preprint at https://doi.org/10.1111/j.1755-5949.2009.00126.x (2010).
72. Fernández-Dueñas, V. *et al.* Revealing Adenosine A(2A)-Dopamine D(2) Receptor Heteromers in Parkinson's Disease Post-Mortem Brain through a New AlphaScreen-Based Assay. *Int J Mol Sci* **20**, 3600 (2019).
73. Fanelli, F., Hanyaloglu, A. C. & Jonas, K. Chapter Five - Integrated structural modeling and super-resolution imaging resolve GPCR oligomers. in *Oligomerization in Health and Disease: From Enzymes to G Protein-Coupled Receptors* (eds. Giraldo, J. & Ciruela, F. B. T.-P. in M. B. and T. S.) vol. 169 151–179 (Academic Press, 2020).
74. Casciari, D., Seeber, M. & Fanelli, F. Quaternary structure predictions of transmembrane proteins starting from the monomer: a docking-based approach. *BMC Bioinformatics* **7**, 340 (2006).
75. Fanelli, F., Seeber, M., Felline, A., Casciari, D. & Raimondi, F. Chapter Five - Quaternary Structure Predictions and Structural Communication Features of GPCR Dimers. in *Oligomerization in Health and Disease* (eds. Giraldo, J. & Ciruela, F. B. T.-P. in M. B. and T. S.) vol. 117 105–142 (Academic Press, 2013).
76. Chen, R., Li, L. & Weng, Z. ZDOCK: An initial-stage protein-docking algorithm. *Proteins: Structure, Function, and Bioinformatics* **52**, 80–87 (2003).

77. Hwang, H., Pierce, B., Mintseris, J., Janin, J. & Weng, Z. Protein–protein docking benchmark version 3.0. *Proteins: Structure, Function, and Bioinformatics* **73**, 705–709 (2008).
78. Sali, A. & Blundell, T. L. Comparative protein modelling by satisfaction of spatial restraints. *J Mol Biol* **234**, 779–815 (1993).
79. Hoare, S. R. J. *et al.* Quantifying the Kinetics of Signaling and Arrestin Recruitment by Nervous System G-Protein Coupled Receptors. *Front Cell Neurosci* **15**, (2022).
80. Henriques, R. *et al.* QuickPALM: 3D real-time photoactivation nanoscopy image processing in ImageJ. *Nat Methods* **7**, 339–340 (2010).

Acknowledgements

We would like to acknowledge Drs Stephen Rothery and David Gaboriau at the Facility for Imaging of Light Microscopy at Imperial College London for their technical support for microscopy experiments. Dr. Asuka Inoue (Univ. Tohoku, Japan) for supplying the β-arrestin1/2 KO cell line. Frederic Jean-Alphonse (CNRS, Nouzilly) for β-arrestin-YFP plasmids, Jonathan Javitch (Univ. Columbia, USA) for WT D_2R plasmids. We would like to acknowledge the use of Biorender.com for the production of schematic figures. This project was funded by Biotechnology and Biological Sciences Research Council (Grant BB/M011178/1).

Author contributions

B.B and A.C.H conceived the study and with K.L.S designed the experiments. K.L.S performed the majority of wet laboratory experiments and analysis with contributions from Y.L for certain βarr BRET recruitment assays and molecular biology; A.J.M for certain cAMP assays; W.Y for some confocal microscopy imaging. F.F performed all molecular modelling and analysis. K.L.S wrote the majority of the manuscript with A.C.H and B.B. F.F wrote the sections of the manuscript relating to molecular modelling, with inputs and review by K.L.S, B.B and A.C.H. All authors contributed to and approved the final manuscript.

Table 1. Quinpirole potency in cAMP and βarr2 BRET recruitment assays shown as $-\log EC_{50}$. Data shown with 95% confidence interval (CI). Two-tailed, unpaired Student's t-test used to determine statistical significance between WT and mutant $-\log EC_{50}$ values (p*=0.0147 (V96C) or 0.0433 (V96S)).

Receptor	**cAMP -log EC_{50}**	**βarr2 recruitment -log EC_{50}**
D_2R WT	-9.554 (CI -9.886 to -9.218)	-5.362 (CI -5.559 to-5.164)
D_2R V96C	-9.106 (CI -9.637 to -8.507)	-5.695 (CI -5.814 to -5.576)*
D_2R V96S	-9.398 (CI -10.04 to -8.747)	-5.804 (CI -6.044 to -5.565)*
D_2R V96S/V97C	-9.367 (-9.808 to -8.899)	-5.622 (-5.788 to -5.457)
D_2R V97C	-9.405 (CI -10.17 to -8.602)	5.626 (CI -5.167 to -6.0850)
D_2R Y93C	-9.464 (-9.840 to -9.078)	5.435 (CI 5.242 to 5.628)

Table 2. Quinpirole- induced βarr2 BRET recruitment kinetics. Rate (k), initial rate, halftime and plateau were calculated following curve fitting from the waveform produced from ligand-induced BRET recruitment assays (Supplementary Fig.6). Data is presented with 3 different D_2R WT data sets, to allow comparisons with mutant D_2R experiments that were carried out at the same time under the same experimental conditions. N=4-6, data shown as +/- SEM. Two-tailed, unpaired Student's t-test used to determine statistical significance between WT and mutant $-\log IC_{50}$ values (p**= 0.0014 or 0.0068).

	k (second-1)	**Initial Rate (BRET ratio units per second)**	**Half time (seconds)**	**Plateau**
WT	1.076×10^{-2} ($\pm 1.283 \times 10^{-3}$)	5.27×10^{-4} ($\pm 1.644 \times 10^{-4}$)	68.38 (±8.537)	0.04908 ($\pm 1.166 \times 10^{-2}$)
V96C	1.999×10^{-2} ($\pm 1.446 \times 10^{-3}$)**	1.002×10^{-3} ($\pm 1.842 \times 10^{-4}$)	35.55 (±3.058)**	0.05012 ($\pm 8.027 \times 10^{-3}$)
WT	4.754×10^{-3} ($\pm 3.549 \times 10^{-3}$)	1.579×10^{-4} ($\pm 1.049 \times 10^{-4}$)	30.28(±4.99)	0.03682 ($\pm 7.335 \times 10^{-3}$)
Y93C	3.33×10^{-3} ($\pm 1.943 \times 10^{-3}$)	1.135×10^{-4} ($\pm 5.866 \times 10^{-5}$)	34.57(±14.05)	0.03119 ($\pm 7.849 \times 10^{-3}$)
V97C	4.434×10^{-3} ($\pm 3.577 \times 10^{-3}$)	1.807×10^{-4} ($\pm 1.499 \times 10^{-4}$)	32.66 (±4.764)	0.0297 ($\pm 6.017 \times 10^{-3}$)
WT	3.065×10^{-2} ($\pm 1.072 \times 10^{-2}$)	8.603×10^{-4} ($\pm 5.241 \times 10^{-4}$)	41.08(± 7.252)	0.02122 ($\pm 5.301 \times 10^{-3}$)
V96S	2.702×10^{-2} ($\pm 8.711 \times 10^{-3}$)	7.002×10^{-4} ($\pm 3.117 \times 10^{-4}$)	39.36 (± 8.69)	0.02394 ($\pm 3.826 \times 10^{-3}$)